THE JOURNAL OF PHYSICAL CHEMISTRY C
A JOURNAL OF THE AMERICAN CHEMICAL SOCIETY

pubs.acs.org/JPCC
Article

Graphene-Enhanced Resonant Arrays of Silver Nanoparticles for Sustained Detection of Raman Signature

Marjan Monshi, Maziar Moussavi, Nadzeya Khinevich, Tomas Tamulevičius, Asta Tamulevičienė, Joel Henzie, Mindaugas Juodėnas,* and Sigitas Tamulevičius*

Cite This: J. Phys. Chem. C 2025, 129, 14983−14992

Read Online

ACCESS | Metrics & More | Article Recommendations | Supporting Information

ABSTRACT: Surface-enhanced Raman Scattering spectroscopy has transformed trace analyte detection by harnessing localized surface plasmon resonance. Hybrid plasmonic−photonic modes have been shown to further improve enhancement factors by tailoring the resonant wavelength. Here, we use a surface lattice resonance-based platform tuned to amplify the Stokes-shifted Raman emission band produced by using capillarity-assisted Ag nanoparticle assembly. Additionally, we transferred graphene onto these substrates to evaluate its effect on the long-term retention of the analyte signal. We monitored the Raman signature of 2-naphthalenethiol on substrates with and without transferred graphene sheets over 1 year since initial exposure. Signal intensities from both the unprotected (U) and graphene-protected (G) samples were projected onto the principal components to evaluate the spectral traits and monitor how the spectra change over time. The results showed that both U and G samples initially exhibited a detection score of approximately 80%. While the U sample completely lost its Raman signal after 300 days, the G sample retained a detection score of about 30%, which remained stable even after 344 days. We attribute the retained signal on the G substrate to two phenomena: (i) graphene prevents the degradation of plasmonic particles and (ii) helps retain the analyte on the substrate. Moreover, the ratio of Raman peaks coinciding with the lattice resonance vs off-resonance peaks was higher compared to a reference measurement. This underscores the potential of graphene−silver hybrid platforms for applications requiring sustained analyte signature, where a long shelf life and prolonged detection over time could facilitate repeated measurements or continuous monitoring without the need for frequent sample replacement on site.

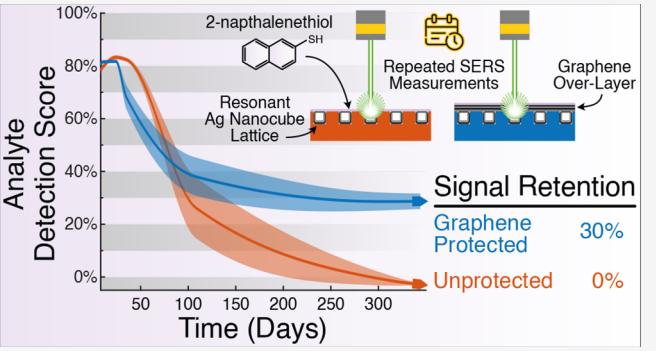

INTRODUCTION

Raman spectroscopy, especially with advancements in surface-enhanced Raman scattering spectroscopy (SERS), has become a preferred analytical technique for identifying and differentiating molecules at low concentrations. This technique, based on the unique material fingerprint of vibrational energy levels, is used across diverse fields, including surface and interface chemistry, catalysis, biology, biomedicine, food science, forensic science, pharmacology, and environmental analysis.[1−6] The continuous drive for greater sensitivity and broader applicability in Raman spectroscopy has encouraged innovations across the field of optical spectroscopy. For instance, in coherent techniques like stimulated Raman scattering microscopy (SRS),[7] advances in instrumentation—particularly in beam shaping and aberration correction—are enabling faster, high-resolution imaging at greater tissue depths. Concurrently, progress in near-field probe design, exemplified by tip-enhanced Raman scattering (TERS),[8] is addressing key limitations such as the weak adsorption of analytes on plasmonic surfaces, thereby enhancing signal strength and spatial resolution. Harnessing this same principle of localized plasmonic enhancement, SERS relies on engineered substrates rather than a single probe.

SERS substrates are typically composed of noble metal nanostructures that support localized surface plasmon resonances (LSPRs)—collective oscillations of conduction electrons excited by an electromagnetic field (EM).[9] Among commonly used metals for SERS substrates, silver (Ag) is the most effective due to its low optical losses and tunable properties enabled by advanced wet-chemistry synthesis techniques.[6,10−13] Strategies to enhance Raman signals using silver-based substrates include the use of diverse supports,[6,14] periodic arrays exploiting surface lattice resonance,[15−17] bimetallic nano shells[18−20] and isolating silver nanoparticles for cross sectional enhancement strategy.[21] Despite these

Received: March 31, 2025
Revised: August 3, 2025
Accepted: August 6, 2025
Published: August 13, 2025

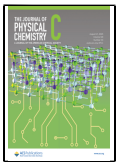

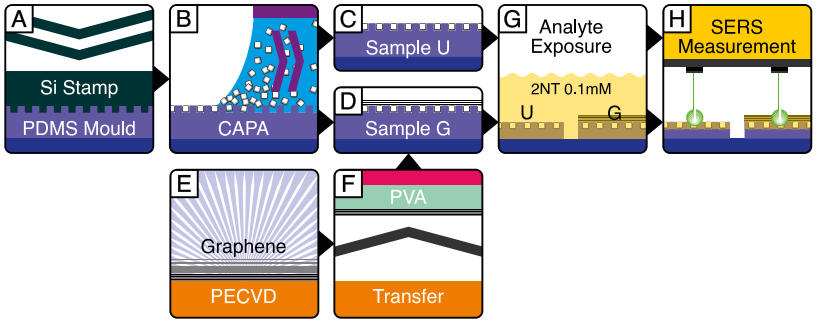

Figure 1. Schematic workflow of the fabrication and analysis process: (A) fabrication of a PDMS substrate by replicating a structured silicon master; (B) deposition of Ag nanoparticles onto the PDMS template using the capillarity-assisted particle assembly (CAPA) method, producing two identical samples (C) and (D); (E) graphene growth on annealed Cu foil via plasma-enhanced chemical vapor deposition (PECVD); (F) graphene transfer onto the Sample G using a lamination method with a poly(vinyl alcohol) (PVA) film; (G) exposure of both samples to the analyte; (H) periodic Raman spectroscopy analysis over time.

advantages, silver is highly susceptible to oxidation and sulfuration, especially when exposed to aqueous environments.[22] Its usage as SERS-active material faces further challenges in terms of producing inexpensive, reproducible, and highly effective substrates.[23] Additionally, the shelf life of SERS substrates is crucial for preserving their sensitivity. If substrates degrade or lose their enhancement properties over time, detection results may become inconsistent and unreliable, even under normal laboratory storage conditions, often due to contamination. To mitigate this issue, substrates that are not inherently protected should undergo additional treatments, such as ion cleaning,[24] to remove surface contaminants like sulfur, chlorine, carbon, and oxygen, which contribute to the degradation of SERS activity.

Graphene−plasmonic hybrid platforms have recently attracted considerable interest as a possible solution to some of the shortcomings.[6,25−29] Graphene, a monolayer of sp^2-bonded carbon atoms arranged in a honeycomb-like structure, has great potential in sensing and biosensing.[30−33] It is also an excellent choice for hybridization with metal nanoparticles to enhance their SERS effect due to its electronic properties, chemical inertness and, more importantly, impermeability.[34] These attributes enable graphene to improve Raman signal detection through mechanisms such as fluorescence quenching,[35] surface passivation, molecule adsorption, and chemical mechanism (CM) enhancement.[28,36,37] Several studies have demonstrated the typical characteristics of CM in graphene-enhanced Raman scattering spectroscopy (GERS) including the first-layer effect, the distance dependence between graphene and analyte molecules,[38−40] the energy alignment between the Fermi level and the highest occupied molecular orbital (HOMO) and lowest unoccupied molecular orbital (LUMO) of the molecule,[41,42] and the influence of molecular orientation.[43] Notably, while the contribution of CM is small compared to that of EM, combining both mechanisms ensures higher SERS performance. It should also be noted that the surface plasmon resonance of graphene lies in the THz region, therefore EM enhancement by graphene itself can be excluded when using excitation in the visible range.[26]

In particular, the protective role of graphene as an overlayer on irregularly distributed silver particles has been highlighted in a few recent studies. Zhang et al.[44] presented a sensitive SERS substrate using a hybrid structure composed of graphene, a silver film, and a laser-textured silicon surface. They showed that the graphene layer reduced SERS signal loss to less than 23% after 50 days of exposure to ambient air compared to significant degradation of substrates without graphene. Osváth et al.[45] synthesized graphene−silver nanoparticle hybrids on highly oriented pyrolytic graphite (HOPG) substrates. They reported that the graphene-covered Ag NPs preserved their LSPR for 3 months, whereas unprotected Ag NPs lost the plasmonic properties completely after 1 month under ambient conditions. Gong et al.[46] have reported graphene-coated Ag nanohole arrays. Nevertheless, although the protective nature of graphene is established, its integration with resonant plasmonic lattices featuring surface lattice resonances remains unexplored, and key questions regarding practical long-term signal stability persist.

Noble metal nanoparticles in periodic arrays exhibit higher resonance Q-factor values ($Q = \lambda/\Delta\lambda = \sim 100$) than single particles ($Q = \sim 5$).[47] This effect, called plasmonic surface lattice resonance (SLR), occurs when the Rayleigh anomaly (RA) spectrally aligns with the LSPR. SLR manifests as a narrow dip in the optical transmission spectrum, which can be tuned via the interplay between the RA and LSPR. Even though the EM field becomes delocalized because of the hybridization with the photonic mode, the overall EM field enhancement in the vicinity of nanoparticles increases.[11,48−50] In SERS, this resonance can be optimized for the Raman measurement[15,17,51,52] with peak enhancement expected when the SLR is between the excitation and Stokes-shifted wavelengths.[53] This has been validated in multiple studies.[54−56] Kerker et al.[57] described this process as (1) enhancement of the incident light at the excitation wavelength and (2) amplification of Raman-scattered photons at the Stokes-shifted wavelength. Kumar et al.[58] confirmed that the EF relates to the product of the squared local field amplitudes at both excitation and emission wavelengths.

In this work, we demonstrate a year-long study of the stability of a graphene-enhanced SERS platform based on assembled periodic arrays of colloidal silver nanoparticles. Our platform is specifically engineered to feature an SLR peak tuned to the Stokes-shifted band of 2-naphthalenethiol (2NT). We employ Principal Component Analysis (PCA) to investigate the influence of graphene as an overlayer and study the evolution of the Raman signal over a year from the initial exposure to the analyte. Our findings suggest how graphene might have a dual role in retaining the SERS signal in such systems. This study is particularly relevant for applications such as environmental monitoring, food safety, and biomedical

https://doi.org/10.1021/acs.jpcc.5c02135
J. Phys. Chem. C 2025, 129, 14983−14992

diagnostics, where enhanced analyte and signal retention can enable prolonged exposure to trace analytes in repeated measurements or continuous monitoring without frequent sample preparation.

MATERIALS AND METHODS

The schematic of the fabrication process of SERS substrates, designated as unprotected (U) and graphene-protected (G), is shown in Figure 1 (see Figure S1 for more details). Each step in the process is detailed in the following sections.

SERS SUBSTRATE FABRICATION

Silver nanocubes were synthesized using a modified polyol method, where polyvinylpyrrolidone (PVP) controlled the shape evolution, yielding monodisperse nanocubes with an average size around 77 ± 3 nm, as detailed elsewhere.[59] The templates for nanoparticle assembly were prepared by molding a structured Si stamp onto a polydimethylsiloxane (PDMS) film via soft-lithography. The silicon master stamp was fabricated using standard lithographic patterning and etching techniques presented in previous work[60] and comprised a 20 mm × 20 mm array of round pillars with a diameter of 180 nm, a height of 100 nm, and periodicity of 400 nm. The nanoparticles were assembled into the templates using capillarity-assisted particle assembly (CAPA).[61] Before deposition, the concentration of the nanoparticles was increased by centrifugation and the solvent was replaced with a 1:2 mixture of ethanol and dimethylformamide (DMF). The polyvinylpyrrolidone (PVP) coating enhanced colloidal stability in DMF.[60] The assembly was performed using a custom-built setup, where a PDMS template was placed on the stage moving at 1 μm/s, and 100 μL of silver nanoparticle suspension was dispensed and confined with a fixed microscope slide. A detailed description of the assembly process can be found in our previous work.[48] Fabricated SERS-active substrates were cleaned with 0.1 M hydrochloric acid for 30 s and then rinsed with ethanol and deionized water to remove the PVP polymer.

GRAPHENE LAYER SYNTHESIS AND TRANSFER

Graphene layers were synthesized using microwave plasma-enhanced chemical vapor deposition (PECVD) with copper foil as the catalytic material.[62] A commercial copper (Cu) foil with a thickness of 45 μm and dimensions of 2 cm × 2 cm was first cleaned by sonication in acetone and isopropanol for 5 min each to remove organic residues. The cleaned foil was then placed in a quartz furnace at atmospheric pressure and subsequently supplied with 200 sccm of pure argon gas (99.9999%). The foil was annealed at 500 °C for 1 h, promoting the formation of Cu_2O layer on the surface. This oxidation plays a crucial role in suppressing the nucleation density of graphene domains, thereby facilitating the growth of larger and more continuous graphene films, which are beneficial for high-quality synthesis.[63]

The Cu foil was then placed in a PECVD chamber on a metal pad featuring a central hole to elevate the foil above the sample holder to maintain a uniform temperature during the synthesis process. Prior to graphene growth, the Cu foil underwent a precleaning step using hydrogen (H_2) plasma at a flow rate of 200 sccm for 30 min under a pressure of 24 mbar. The plasma power was 1.1 kW, while a constant temperature of 550 °C was maintained solely through microwave induction and plasma-species collisions, without any additional heating. Following precleaning, graphene growth was initiated by introducing methane (CH_4) as a carbon source at a flow rate of 25 sccm, while keeping all other parameters unchanged. After a 10 min growth stage, the plasma was turned off, allowing the system to cool down naturally. The device returned to room temperature over a period of approximately 2 h.

The synthesized graphene-coated Cu foil was then extracted for subsequent transfer and further characterization. Commercial water-soluble poly(vinyl alcohol) (PVA) films with paper backing were used for graphene transfer from the copper foil to SERS substrate. The PVA film was laminated onto the graphene-coated copper foil using a commercial hot-roll laminator at 110 °C and operated at low speed to prevent bubbling. The laminated foil was then baked on a preheated hot plate at 110 °C to enhance adhesion between the PVA film and graphene. The PVA film, along with the graphene, was detached from the copper foil and carefully laminated onto the SERS substrate with assembled nanoparticles several times. The paper backing was then removed, and the PVA was dissolved by immersing the substrate in deionized water overnight at room temperature.[64] This specific set of transfer parameters was found to provide an effective balance between maintaining the structural integrity of the graphene layer and achieving sufficient conformal adhesion to the topographically patterned PDMS substrate.

CHARACTERIZATION TECHNIQUES

The UV−vis transmittance spectra of the fabricated array of nanoparticles on the patterned PDMS substrate were measured using an optical fiber-coupled spectrometer (AvaSpec-2048, Avantes; resolution 1.2 nm) and a custom-made collimated light source covering the 400−800 nm range.[65]

2NT, a simple aromatic molecule with an extended π-conjugated system, was used to evaluate the long-term retention of its Raman signal on two SERS substrates (U and G) after immersion in a 10^{-4} M solution. SERS measurements were conducted using a Raman microscope equipped with a thermoelectrically cooled CCD detector, InVia (Renishaw). Measurements were performed using a 532 nm laser excitation source at 0.3 mW power, with an exposure time of 60 s and a 50× objective lens (other measurement parameters are listed in Table S1 in the Supporting Information). The U and G samples were measured at eight time points: immediately after exposure and after 10, 16, 24, 35, 108, 303, and 344 days. Reference samples of pure 2NT, PDMS, and graphene were also measured to establish a reference data set for evaluation purposes.

DATA ANALYSIS

To systematically analyze the Raman scattering data (range: 480−1650 cm^{-1}) and evaluate the spectral characteristics, a multistep data processing workflow was implemented. The Raman spectra from each sample were imported and preprocessed using a custom MATLAB script. Noise in the raw spectra was mitigated using a Savitzky−Golay filter to enhance signal clarity. The spectral baseline was corrected using a nonquadratic asymmetric Huber function,[66] which effectively removes broad, nonspecific background signals while preserving analyte-specific Raman signatures. Unlike traditional least-squares estimation, which minimizes a quadratic cost function, the Huber function minimizes a

https://doi.org/10.1021/acs.jpcc.5c02135
J. Phys. Chem. C 2025, 129, 14983−14992

nonquadratic cost function, offering a more robust solution for this type of spectral data.

All spectra were normalized by dividing the intensity values by the Euclidean norm of the spectral vector to ensure comparability across data sets. The spectra were then interpolated to a common Raman shift range, enabling a consistent data alignment for multivariate analysis. Reference spectra (collected from pure crystalline 2NT, the PDMS substrate, and graphene layers) were analyzed by using Principal Component Analysis (PCA) to extract principal components (PCs) that capture dominant variance patterns across the distinct signatures of the reference materials. Raman spectra from both the U and G samples at various time points were projected onto the PCs derived from the reference spectra. See the Supporting Information for more details on the PCA method.

RESULTS AND DISCUSSION

Characteristics of SERS Substrate. SERS enhancement on a resonant lattice is primarily governed by the spectral positioning of the SLR. Here, we selectively target the Stokes-shifted scattering wavelengths of 2NT in the range of 811−1556 cm^{-1}. For the wavelength of the used excitation laser (532 nm), this range of Raman shifts corresponds to 556−580 nm. The RA wavelength at normal incidence for a square grating in PDMS is defined by $\lambda_{RA} = \Lambda \times n$. The SLR closely follows the RA, provided that the individual nanoparticle dipolar LSPR is blue-shifted with respect to it. Therefore, the condition for targeted SERS enhancement can be expected using a 400 nm square grating in PDMS (Λ = 400 nm, refractive index, $n \simeq 1.4$), where the RA wavelength is ∼560 nm.[15,48,67]

Figure 2A shows the UV−vis extinction spectrum of the periodic arrays of silver nanoparticles on PDMS measured at normal incidence following assembly. The spectrum exhibits two distinct peaks: a broad peak around 430 nm and a sharper peak near 570 nm. The broad peak corresponds to the quadrupolar LSPR of the individual silver nanoparticles. The dipolar LSPR, although imperceptible in the spectrum, hybridizes with the photonic RA mode[67] and appears as a sharp SLR peak at ∼570 nm, matching the wavelength range for the amplification of 2NT signal. Figure 2B presents an SEM micrograph of the assembled plasmonic structure. The uniformity of the traps in the patterned substrate ensures a consistent spacing and geometry across the array, contributing to the reproducibility and scalability of the plasmonic substrate.

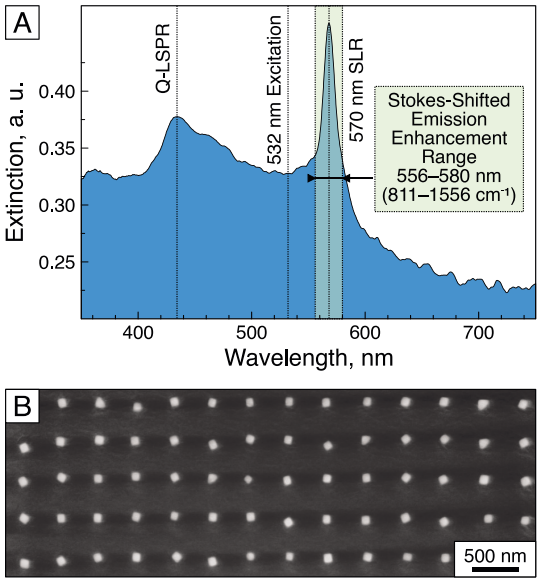

Figure 2. (A) UV−vis extinction spectrum of periodic arrays of silver nanoparticles on PDMS, measured at normal incidence following initial deposition. (B) Scanning electron microscopy (SEM) image of nanoparticle (NP) arrays on PDMS.

Raman Scattering Spectroscopy. Figure 3 presents the Raman spectrum of graphene used in this study. Seven bands have been identified in the spectrum: four prominent bands in the first-region (D, G, D′, and 2D bands) and three less-prominent bands in the second-order region (G*, D+D′, and 2D′ bands). The spectral positions and other specifications of these bands are listed in Table 1.

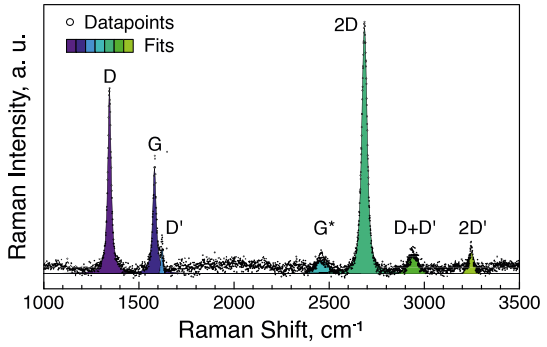

Figure 3. A representative Raman spectrum of the reference graphene sample on copper foil with fitted bands overlaid.

Table 1. Fitting Results for the Graphene Reference Sample Obtained Using the 7-Band Fitting Model

Band	Center (cm^{-1})	FWHM (cm^{-1})	Intensity	Fit Type
D	1345.1	20.8	1.76	Voigt
G	1581.6	21.8	1.00	Voigt
D′	1621.9	15.0	0.24	Gaussian
G*	2461.2	95.0	0.13	Gaussian
2D	2685.5	33.8	2.34	Voigt
D+D′	2940.8	76.1	0.17	Gaussian
2D′	3244.9	45.2	0.20	Gaussian

The D band corresponds to phonons activated only in disordered structures and is associated with sp^2 hybridization from double resonance scattering. The G band arises from single-resonance vibrations of the in-plane E_{2g} mode, representing the planar sp^2-bonded carbon configuration. The D′ band represents a double resonance mode activated by a disordered graphitic lattice, with its intensity increasing as more defects are introduced.

The Raman spectrum in Figure 3 confirms the synthesis of single-layer graphene with a significant density of structural defects. The definitive evidence for a monolayer is the 2D peak, which is sharp, symmetric, and well-fitted by a single Voigt function with a FWHM of ∼34 cm^{-1}. This conclusion is further supported by the high $I_{2D/G}$ intensity ratio of ∼2.68.[68] The high $I_{D/G}$ ratio of ∼2.2 suggests a high concentration of defects, which is expected from a low-temperature growth

https://doi.org/10.1021/acs.jpcc.5c02135
J. Phys. Chem. C 2025, 129, 14983−14992

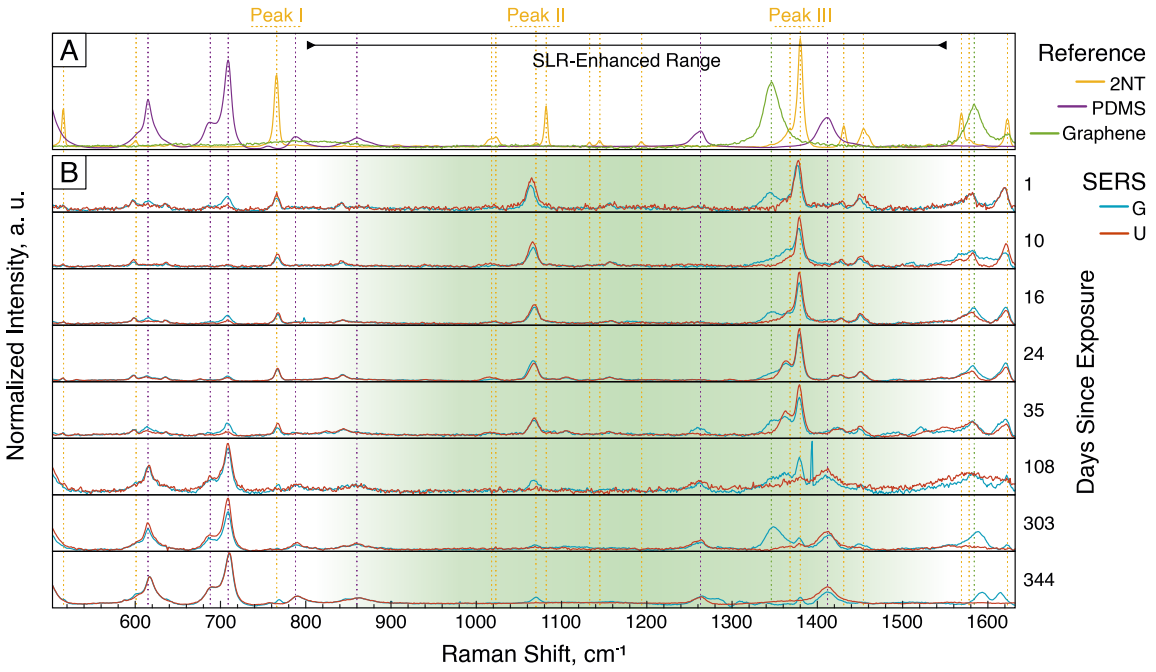

Figure 4. (A) Averaged and normalized Raman spectra for reference samples: graphene (green), PDMS (purple), and 2NT (yellow), with vertical lines indicating characteristic peak positions. Peaks I, II, and III mark the 2NT peaks used for selective amplification analysis. (B) The temporal evolution of Raman spectra for 2NT on SERS substrates on sample G in blue and sample U in orange, recorded over a period from day 1 to day 344 since initial exposure to the analyte. The shaded region marks the SLR-enhanced range.

Table 2. Normalized Intensities and Calculated Enhancement Factors (EFs) for Characteristic Raman Peaks of 2NT[a]

Peak	Position (cm^{-1}) (Reference)	Normalized Intensity (Reference)	Normalized Intensity (SERS)	Enhancement Factor (EF)
I (off resonance)	766	1	1	x1
II (on resonance)	1082	0.38 ± 0.03	3.39 ± 0.16	x8.92 ± 0.78
III (on resonance)	1380	1.92 ± 0.11	6.80 ± 0.30	x3.54 ± 0.26

[a]Peak I (766 cm^{-1}), located outside the SLR range, serves as the normalization reference.

process and is likely related to vacancies and nonuniform grain boundaries. These structural defects can also be responsible for other observed spectral features in highly disordered systems. The G band position,[69] less prominent bands in the second-order region (2300−3300 cm^{-1}),[70] and the G* band[71] can sometimes be associated with multiple layers, but here we attribute them to defect-induced compressive strain and/or unintentional doping.

Figure 4 presents the averaged Raman spectra obtained from measurements of the reference samples, including PDMS, graphene, and 2NT molecules (Figure 4A), along with the temporal evolution of SERS measurements on U and G substrates over time (Figure 4B). Measurements were performed immediately after exposure to the analyte and after 10, 16, 24, 35, 108, 303, and 344 days. It is important to mention that the substrates were not repeatedly exposed to the analyte for every measurement. Vertical lines in the figure indicate characteristic peak positions within the Raman shift range from 480 to 1650 cm^{-1}.

The PDMS reference spectrum exhibits distinct peaks at 490, 612, 705, 1260, and 1410 cm^{-1}.[15,72] The 2NT molecule peaks are observed at 515, 599, 766, and 1020 cm^{-1} which correspond to ring deformation and C−H bending, 1082 cm^{-1} associated with ring breathing coupled with C−S stretching and in-plane C−H bending, 1380 cm^{-1} representing the D-mode of the aromatic rings, 1433 and 1455 cm^{-1} attributed to in-plane C−H bending coupled with ring C═C stretching and C−S stretching, and 1570 and 1622 cm^{-1} corresponding to the characteristic C═C stretching modes of the aromatic ring.

SLR-Based SERS Enhancement. To assess the enhancement provided by our SERS substrates, we analyzed three relatively dominant and isolated characteristic Raman peaks of the 2NT: Peak I at approximately 766 cm^{-1}, Peak II at 1082 cm^{-1}, and Peak III at 1380 cm^{-1} (see Figure S2). Peak I lies outside the SLR enhancement range, which is expected to remain unaffected by the SLR and thus serves as an internal reference, whereas Peaks II and III are positioned within the SLR resonance region (556−580 nm). These latter peaks are expected to be selectively enhanced by the SLR effect.

Gaussian peak fitting was applied to both the 2NT reference and the SERS spectra from both U and G samples obtained during the initial month, providing normalized peak intensities relative to Peak I. The calculated enhancement factors reflect selective amplification of Peaks II and III under SERS conditions (Table 2). The comparison clearly illustrates the relative increase in intensity for Peaks II and III, suggesting that their enhancement correlates directly with the position of the SLR peak.

Principal Component Analysis. The Raman spectral data of the reference samples were subjected to PCA to identify the patterns of variance. It is important to note that Raman analysis often relies on relative peak intensity ratios or peak fitting to derive metrics. However, these methods struggle with overlapping peaks and trace concentrations, as they reduce the

https://doi.org/10.1021/acs.jpcc.5c02135
J. Phys. Chem. C 2025, 129, 14983−14992

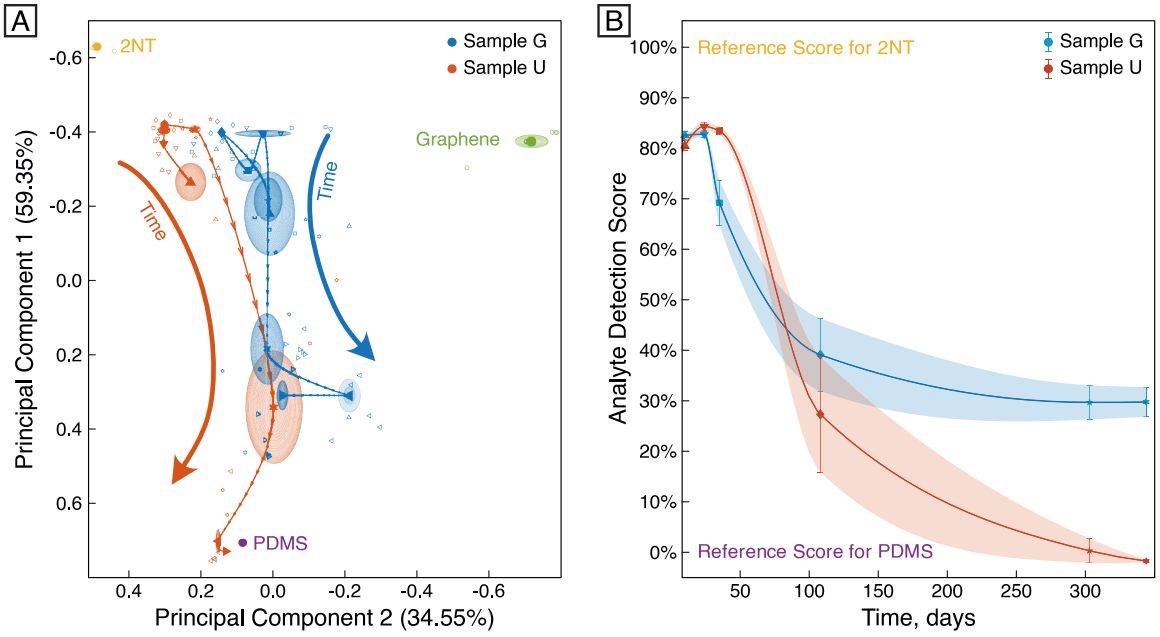

Figure 5. (a) PCA score plot showing the clustering of reference signatures (2NT, PDMS, and graphene) and the intermediate positions of SERS observations from samples U and G over time. PC1 (59.35% variance) separates the 2NT and PDMS reference signatures, while PC2 (34.55% variance) mainly captures the graphene signature. Standard error bands (shaded regions) illustrate the variability of mean scores. (b) Analyte detection scores (based on normalized PC1) for samples U and G as a function of time. Detection scores for sample U decline from 70 to 80% initially to 30% by day 108 and become indistinguishable from PDMS after 300 days. In contrast, sample G retains ∼40% of its initial detection score after 100 days, stabilizing at ∼29.7%.

spectral data set to a single parameter, leading to a loss of critical information.[73] PCA addresses these challenges by leveraging the entire spectral data set, capturing both prominent and subtle variations, and generating a set of robust metrics known as principal components (PCs). By plotting our observation points against the first two principal components in Figure 5A, we visualized 95% of the variance in the high-dimensional spectral data set, with PC1 capturing ∼60% and PC2 accounting for ∼35% of the variance. The scree plot (Figure S3) confirms that PC1 and PC2 together explain nearly 94% of the total variance, with an elbow point at PC3, justifying the selection of the first two components for spectral differentiation.

Distinct clustering of the reference samples for PDMS (+0.7 on PC1) and 2NT (−0.65 on PC1) clearly separates their Raman signatures. Within this PCA space, the measurements taken on the SERS substrate span intermediate positions from −0.4 to +0.6 on PC1, reflecting the relative contributions of PDMS and 2NT in the spectra. This projection effectively illustrates the relative concentration of each reference signature. Observations with stronger 2NT signature cluster near the 2NT reference (−0.4 < PC1 < −0.2), while those dominated by PDMS signature shift toward positive PC1 scores, closer to the PDMS reference. These findings confirm PC1 as a reliable metric for evaluating the relative concentration of 2NT vs the PDMS background. The second principal component (PC2) primarily distinguishes the graphene signature at PC2 = −0.7 from the other two references with positive scores. As a result, SERS spectra from sample G align more closely with the graphene reference compared to the U series.

By normalizing PC1 scores linearly, we created a quantitative score for analyte detection ranging from 0% (no 2NT detected) to 100% (pure 2NT detected). We used this metric to track the time-dependent evolution of the SERS signal, as illustrated in Figure 5B. Results revealed that both U and G samples initially showed a detection score of around 80%. After 300 days, the U sample completely lost the Raman signal, while the G sample still exhibited a detection score of approximately 30% and retained it after 344 days. The decay curve for the U sample follows a trend that can be approximated by an exponential decay, a pattern consistent with first-order kinetic processes that often govern material degradation and analyte desorption.

It should be noted that PCA has limitations, particularly in handling nonlinear combinations of components or variations in spectral characteristics. For instance, variations in graphene's D/G ratio across observations result in shifts in PC2, with some observations from the G sample moving further from the graphene reference. Peak shifts or new peaks emerging from molecular bonding can also reduce PCA's sensitivity, as demonstrated by the 2NT peak shifting from 1080 cm^{-1} in its crystalline form (reference) to 1070 cm^{-1} on the SERS substrate.[74] Despite these challenges, PCA proved effective by detecting the 2NT signal (Detection Score = 30%) in sample U at Day 108, even when the isolated 1070 cm^{-1} band was no longer detectable (Supplementary Figure S4). This underscores PCA's capability compared to manual peak-fitting methods for generalized spectral analysis and long-term monitoring.

DISCUSSION

The results indicate that during the first month, the detection score remained relatively stable and even higher for sample U. This observation aligns with the findings of Gong et al.,[46] who reported a slightly higher enhancement factor for bare metal substrates. This effect can be attributed to the additional distance introduced by graphene layers compared with the

https://doi.org/10.1021/acs.jpcc.5c02135
J. Phys. Chem. C 2025, 129, 14983−14992

direct interaction between analyte molecules and metal particles. Over time, however, both samples exhibited a decline in the signal intensity. While the detection score for sample G stabilized at approximately 29.7%, the score of sample U dropped to zero. The decline is primarily due to oxidation and sulfurization,[45] which degrades nanoparticles directly exposed to the analyte and ambient air. In our study, this degradation was further intensified by the strong chemisorption between the thiol (-SH) groups of 2NT and the silver surface, initiating chemical reactions that progressively deteriorated the plasmonic properties and, in turn, promoted analyte desorption, leading to a complete loss of the SERS effect in U samples under a natural atmosphere.

Despite some degradation in sample G due to inhomogeneous graphene coverage and defects introduced during transfer, the sample retained detectable spectral features of the 2NT over extended periods. We attribute this stabilization to two key factors: (1) physical barrier effect and (2) enhanced adsorption equilibrium. In regions of complete coverage, the impermeable graphene layer shields the silver nanoparticles from ambient air and the analyte solution, preventing the oxidative and chemical degradation that leads to the loss of plasmonic properties.[45] Second, graphene provides a stable surface for analyte retention through $\pi-\pi$ stacking. This interaction, which is strongest when the aromatic rings of 2-NT are oriented parallel to the graphene surface, alters the long-term adsorption/desorption equilibrium.[75] Although $\pi-\pi$ stacking interaction is weaker compared to covalent bonds formed by thiol groups with metal particles, they are still significant when the substrate is an aromatic system like graphene.[76,77] Moreover, it has been shown that the presence of defects facilitates better attachment of probe molecules.[78] Smith and Kay[79] demonstrated that benzene remains adsorbed on graphene surfaces via van der Waals interactions, exhibiting first-order desorption kinetics. Similarly, Chakradhar et al.[80] showed that while the interaction strength between benzene and graphene can be modulated by the underlying substrate, it remains sufficiently robust to delay desorption. These two mechanisms result in a stable, long-term population of adsorbed molecules, explaining the sustained SERS signal on sample G, in stark contrast to the complete signal loss on the U sample, where the degrading silver surface could no longer retain the analyte.

CONCLUSIONS

In this work, we investigated the year-long stability of a graphene-protected SERS platform based on resonant silver nanoparticle arrays and suggested mechanisms responsible for signal retention. We demonstrated an efficient approach for fabricating plasmonic SERS substrates with a dry-transferred graphene overlayer. We followed the SERS signal kinetics of 2NT spectra on unprotected (U) and graphene-covered (G) SERS substrates over 344 days and used Principal Component Analysis to evaluate performance. Over time, both samples exhibited a decline in signal intensity, but the detection score for the G sample stabilized at approximately 29.7%, while the score for the U sample dropped to zero. This stabilization can be attributed to two key factors: (1) the protective effect of graphene, shielding silver nanoparticles from ambient air and analyte exposure, and (2) enhanced analyte retention via $\pi-\pi$ stacking interactions.

These graphene-protected substrates show significant promise for applications requiring long-term stability, such as continuous environmental and biomedical monitoring. Future work could focus on optimizing the trade-off between initial sensitivity and longevity by improving graphene transfer uniformity or engineering nanoparticle-graphene spacing. Furthermore, the fabrication and transfer methodology presented here could be adapted to integrate other 2D materials, opening new possibilities for the design of hybrid sensors with tailored properties.

ASSOCIATED CONTENT

Supporting Information

The Supporting Information is available free of charge at https://pubs.acs.org/doi/10.1021/acs.jpcc.5c02135.

Detailed workflow of the fabrication and analysis process (Figure S1); details on the Principal Component Analysis (PCA) methodology; comparison of average Raman spectra normalized to the intensity of Peak I (Figure S2); scree plot showing the variance explained by each principal component (PC) in the Raman spectral data set (Figure S3); Raman measurement settings (Table S1); evolution of the normalized peak intensity at 1067 cm^{-1} for the U and G SERS samples over time (Figure S4) (PDF)

AUTHOR INFORMATION

Corresponding Authors

Mindaugas Juodėnas − *Institute of Materials Science, Kaunas University of Technology, LT-51423 Kaunas, Lithuania;* orcid.org/0000-0002-0517-8620; Email: mindaugas.juodenas@ktu.lt

Sigitas Tamulevičius − *Institute of Materials Science, Kaunas University of Technology, LT-51423 Kaunas, Lithuania; Department of Physics, Kaunas University of Technology, Kaunas LT-51368, Lithuania;* orcid.org/0000-0002-9965-2724; Email: sigitas.tamulevicius@ktu.lt

Authors

Marjan Monshi − *Institute of Materials Science, Kaunas University of Technology, LT-51423 Kaunas, Lithuania*

Maziar Moussavi − *Institute of Materials Science, Kaunas University of Technology, LT-51423 Kaunas, Lithuania;* orcid.org/0000-0003-4108-9454

Nadzeya Khinevich − *Institute of Materials Science, Kaunas University of Technology, LT-51423 Kaunas, Lithuania;* orcid.org/0000-0001-9348-3918

Tomas Tamulevičius − *Institute of Materials Science, Kaunas University of Technology, LT-51423 Kaunas, Lithuania; Department of Physics, Kaunas University of Technology, Kaunas LT-51368, Lithuania;* orcid.org/0000-0003-3879-2253

Asta Tamulevičienė − *Institute of Materials Science, Kaunas University of Technology, LT-51423 Kaunas, Lithuania; Department of Physics, Kaunas University of Technology, Kaunas LT-51368, Lithuania;* orcid.org/0000-0003-4152-1382

Joel Henzie − *Research Center for Materials Nanoarchitectonics (MANA), National Institute for Materials Science (NIMS), Tsukuba, Ibaraki 305-0044, Japan;* orcid.org/0000-0002-9190-2645

Complete contact information is available at: https://pubs.acs.org/10.1021/acs.jpcc.5c02135

Notes

The authors declare no competing financial interest.

■ ACKNOWLEDGMENTS

The research was implemented within the NANOTRAACES project carried out under the M-ERA.NET 2 scheme. This project has received funding from the Research Council of Lithuania (LMTLT), agreement No MERANET-22-2.

■ REFERENCES

(1) Zheng, X.; Ye, Z.; Akmal, Z.; He, C.; Zhang, J.; Wang, L. Recent Progress in SERS Monitoring of Photocatalytic Reactions. *Chem. Soc. Rev.* **2024**, *53* (2), 656−683.
(2) Karlo, J.; Razi, S. S.; Phaneeswar, M. S.; Vijay, A.; Singh, S. P. Metallic Nanoparticles for Surface-Enhanced Raman Scattering Based Biosensing Applications. *Photochem* **2024**, *4* (4), 417−433.
(3) Moldovan, R.; Vereshchagina, E.; Milenko, K.; Iacob, B. C.; Bodoki, A. E.; Falamas, A.; Tosa, N.; Muntean, C. M.; Farcău, C.; Bodoki, E. Review on Combining Surface-Enhanced Raman Spectroscopy and Electrochemistry for Analytical Applications. *Anal. Chim. Acta* **2022**, *1209*, 339250.
(4) Srivastava, S.; Wang, W.; Zhou, W.; Jin, M.; Vikesland, P. J. Machine Learning-Assisted Surface-Enhanced Raman Spectroscopy Detection for Environmental Applications: A Review. *Environ. Sci. Technol.* **2024**, *58* (47), 20830−20848.
(5) Cao, Y.; Cheng, Y.; Sun, M. Graphene-Based SERS for Sensor and Catalysis. *Appl. Spectrosc. Rev.* **2023**, *58* (1), 1−38.
(6) Tong, Q.; Wang, W.; Fan, Y.; Dong, L. Recent Progressive Preparations and Applications of Silver-Based SERS Substrates. *TrAC Trends in Analytical Chemistry* **2018**, *106*, 246−258.
(7) Wang, W.; Huang, Z.; Pirone, D.; Sirico, D.; Miccio, L.; Bianco, V.; Mugnano, M.; Del Giudice, D.; Pasquinelli, G.; Valente, S.; et al. Stimulated Raman Scattering Microscopy with Phase-Controlled Light Focusing and Aberration Correction for Rapid and Label-Free, Volumetric Deep Tissue Imaging. *Opto-Electronic Advances* **2024**, *7* (9), 240064.
(8) Xie, Z.; Meng, C.; Yue, D.; Xu, L.; Mei, T.; Zhang, W. Tip-Enhanced Raman Scattering of Glucose Molecules. *Opto-Electronic Science* **2025**, *4* (5), 240027.
(9) Han, X. X.; Rodriguez, R. S.; Haynes, C. L.; Ozaki, Y.; Zhao, B. Surface-Enhanced Raman Spectroscopy. *Nature Reviews Methods Primers* **2021**, *1* (1), 1−17.
(10) Li, Y.; Liao, Q.; Hou, W.; Qin, L. Silver-Based Surface Plasmon Sensors: Fabrication and Applications. *International Journal of Molecular Sciences* **2023**, *24* (4), 4142.
(11) Deng, S.; Li, R.; Park, J. E.; Guan, J.; Choo, P.; Hu, J.; Smeets, P. J. M.; Odom, T. W. Ultranarrow Plasmon Resonances from Annealed Nanoparticle Lattices. *Proc. Natl. Acad. Sci. U. S. A.* **2020**, *117* (38), 23380−23384.
(12) Juodėnas, M.; Peckus, D.; Tamulevičius, T.; Yamauchi, Y.; Tamulevičius, S.; Henzie, J.; Henzie, J. Effect of Ag Nanocube Optomechanical Modes on Plasmonic Surface Lattice Resonances. *ACS Photonics* **2020**, *7* (11), 3130−3140.
(13) Rycenga, M.; Cobley, C. M.; Zeng, J.; Li, W.; Moran, C. H.; Zhang, Q.; Qin, D.; Xia, Y. Controlling the Synthesis and Assembly of Silver Nanostructures for Plasmonic Applications. *Chem. Rev.* **2011**, *111* (6), 3669−3712.
(14) Khinevich, N.; Juodėnas, M.; Tamulevičienė, A.; Bandarenka, H.; Tamulevičius, S. Tailoring Mesoporous Silicon Surface to Form a Versatile Template for Nanoparticle Deposition. *Coatings* **2021**, *11* (6), 699.
(15) Khinevich, N.; Juodėnas, M.; Tamulevičienė, A.; Tamulevičius, T.; Talaikis, M.; Niaura, G.; Tamulevičius, S. Wavelength-Tailored Enhancement of Raman Scattering on a Resonant Plasmonic Lattice. *Sens Actuators B Chem.* **2023**, *394*, 134418.
(16) Ragheb, I.; Braïk, M.; Lau-Truong, S.; Belkhir, A.; Rumyantseva, A.; Kostcheev, S.; Adam, P. M.; Chevillot-Biraud, A.; Lévi, G.; Aubard, J.; et al. Surface Enhanced Raman Scattering on Regular Arrays of Gold Nanostructures: Impact of Long-Range Interactions and the Surrounding Medium. *Nanomaterials* **2020**, *10* (11), 2201.
(17) Alam, K.; Kabusure, K. M.; Asamoah, B. O.; Nuutinen, T.; Baah, M.; Mohamed, S.; Matikainen, A.; Heikkinen, J.; Rekola, H.; Roussey, M.; et al. Double Resonant Plasmonic Lattices for Raman Studies. *Nanoscale* **2020**, *12* (45), 23166−23172.
(18) Alvarez-Puebla, R. A.; Ross, D. J.; Nazri, G. A.; Aroca, R. F. Surface-Enhanced Raman Scattering on Nanoshells with Tunable Surface Plasmon Resonance. *Langmuir* **2005**, *21* (23), 10504−10508.
(19) Wang, L.; Wang, E.; Tang, J. Facile Synthesis of Flower-like Ag Nanocube@mesoporous SiO2 and Their Sensitive SERS Performance. *J. Nanopart. Res.* **2019**, *21* (3), 1−7.
(20) Zhang, H.; Song, D.; Gao, S.; Zhang, J.; Zhang, H.; Sun, Y. Novel SPR Biosensors Based on Metal Nanoparticles Decorated with Graphene for Immunoassay. *Sens Actuators B Chem.* **2013**, *188*, 548−554.
(21) Cao, Z.; He, P.; Huang, T.; Yang, S.; Han, S.; Wang, X.; Ding, G. Plasmonic Coupling of AgNPs near Graphene Edges: A Cross-Section Strategy for High-Performance SERS Sensing. *Chem. Mater.* **2020**, *32* (9), 3813−3822.
(22) Sultan, M. F. An Investigation of the Influence of the Graphene Layers Number on the Performance of Surface Plasmon Resonance Biosensors with Various Thicknesses of Silver. *J. Opt* **2024**, *53* (5), 4893−4900.
(23) Pérez-Jiménez, A. I.; Lyu, D.; Lu, Z.; Liu, G.; Ren, B. Surface-Enhanced Raman Spectroscopy: Benefits, Trade-Offs and Future Developments. *Chem. Sci.* **2020**, *11* (18), 4563−4577.
(24) Nuntawong, N.; Eiamchai, P.; Wong-Ek, B.; Horprathum, M.; Limwichean, K.; Patthanasettakul, V.; Chindaudom, P. Shelf Time Effect on SERS Effectiveness of Silver Nanorod Prepared by OAD Technique. *Vacuum* **2013**, *88* (1), 23−27.
(25) Zhang, Z.; Lee, Y.; Haque, M. F.; Leem, J.; Hsieh, E. Y.; Nam, S. W. Plasmonic Sensors Based on Graphene and Graphene Hybrid Materials. *Nano Convergence* **2022**, *9* (1), 28.
(26) Lin, J.; Zhang, N.; Tong, L.; Zhang, J. Enhanced Raman Scattering on Graphene and Beyond. *Frontiers of Plasmon Enhanced Spectroscopy Vol. 2*; ACS Symposium Series; American Chemical Society, 2016; No. 1246, pp 97−119, DOI: 10.1021/bk-2016-1246.ch005.
(27) Zhang, N.; Tong, L.; Zhang, J. Graphene-Based Enhanced Raman Scattering toward Analytical Applications. *Chem. Mater.* **2016**, *28* (18), 6426−6435.
(28) Lai, H.; Xu, F.; Zhang, Y.; Wang, L. Recent Progress on Graphene-Based Substrates for Surface-Enhanced Raman Scattering Applications. *J. Mater. Chem. B* **2018**, *6* (24), 4008−4028.
(29) Zhang, N.; Tong, L.; Zhang, J. Graphene-Based Enhanced Raman Scattering toward Analytical Applications. *Chem. Mater.* **2016**, *28* (18), 6426−6435.
(30) Pourmadadi, M.; Dinani, H. S.; Tabar, F. S.; Khassi, K.; Janfaza, S.; Tasnim, N.; Hoorfar, M. Properties and Applications of Graphene and Its Derivatives in Biosensors for Cancer Detection: A Comprehensive Review. *Biosensors* **2022**, *12* (5), 269.
(31) Bhatt, S.; Punetha, V. D.; Pathak, R.; Punetha, M. Two-Dimensional Carbon Nanomaterial-Based Biosensors: Micromachines for Advancing the Medical Diagnosis. *Advanced Structured Materials* **2023**, *190*, 181−225.
(32) Cao, Y.; Cheng, Y.; Sun, M. Graphene-Based SERS for Sensor and Catalysis. *Appl. Spectrosc Rev.* **2023**, *58* (1), 1−38.
(33) Zhao, Y.; Li, X. G.; Zhou, X.; Zhang, Y. N. Review on the Graphene Based Optical Fiber Chemical and Biological Sensors. *Sens Actuators B Chem.* **2016**, *231*, 324−340.
(34) Bunch, J. S.; Verbridge, S. S.; Alden, J. S.; Van Der Zande, A. M.; Parpia, J. M.; Craighead, H. G.; McEuen, P. L. Impermeable Atomic Membranes from Graphene Sheets. *Nano Lett.* **2008**, *8* (8), 2458−2462.
(35) Xie, L.; Ling, X.; Fang, Y.; Zhang, J.; Liu, Z. Graphene as a Substrate to Suppress Fluorescence in Resonance Raman Spectroscopy. *J. Am. Chem. Soc.* **2009**, *131* (29), 9890−9891.

(36) Zhou, Q.; Jin, M.; Wu, W.; Fu, L.; Yin, C.; Karimi-Maleh, H. Graphene-Based Surface-Enhanced Raman Scattering (SERS) Sensing: Bibliometrics Based Analysis and Review. *Chemosensors 2022, Vol. 10, Page 317* **2022**, *10* (8), 317.
(37) Nurrohman, D. T.; Chiu, N. F. A Review of Graphene-Based Surface Plasmon Resonance and Surface-Enhanced Raman Scattering Biosensors: Current Status and Future Prospects. *Nanomaterials* **2021**, *11* (1), 216.
(38) Ling, X.; Xie, L.; Fang, Y.; Xu, H.; Zhang, H.; Kong, J.; Dresselhaus, M. S.; Zhang, J.; Liu, Z. Can Graphene Be Used as a Substrate for Raman Enhancement? *Nano Lett.* **2010**, *10* (2), 553−561.
(39) Ling, X.; Zhang, J. First-Layer Effect in Graphene-Enhanced Raman Scattering. *Small* **2010**, *6* (18), 2020−2025.
(40) Dai, Z. G.; Xiao, X. H.; Wu, W.; Zhang, Y. P.; Liao, L.; Guo, S. S.; Ying, J. J.; Shan, C. X.; Sun, M. T.; Jiang, C. Z. Plasmon-Driven Reaction Controlled by the Number of Graphene Layers and Localized Surface Plasmon Distribution during Optical Excitation. *Light: Science & Applications* **2015**, *4* (10), No. e342.
(41) Xu, H.; Xie, L.; Zhang, H.; Zhang, J. Effect of Graphene Fermi Level on the Raman Scattering Intensity of Molecules on Graphene. *ACS Nano* **2011**, *5* (7), 5338−5344.
(42) Xu, H.; Chen, Y.; Xu, W.; Zhang, H.; Kong, J.; Dresselhaus, M. S.; Zhang, J. Modulating the Charge-Transfer Enhancement in GERS Using an Electrical Field under Vacuum and an n/p-Doping Atmosphere. *Small* **2011**, *7* (20), 2945−2952.
(43) Ling, X.; Wu, J.; Xu, W.; Zhang, J. Probing the Effect of Molecular Orientation on the Intensity of Chemical Enhancement Using Graphene-Enhanced Raman Spectroscopy. *Small* **2012**, *8* (9), 1365−1372.
(44) Zhang, C.; Lin, K.; Huang, Y.; Zhang, J. Graphene-Ag Hybrids on Laser-Textured Si Surface for SERS Detection. *Sensors* **2017**, *17* (7), 1462.
(45) Osváth, Z.; Pálinkás, A.; Piszter, G.; Molnár, G. Synthesis and Characterization of Graphene-Silver Nanoparticle Hybrid Materials. *Materials* **2020**, *13* (20), 4660.
(46) Gong, T.; Luo, Y.; Zhao, C.; Yue, W.; Zhang, J.; Zhu, Y.; Pu, M.; Zhang, Z.; Wang, C.; Luo, X. Highly Reproducible and Stable Surface-Enhanced Raman Scattering Substrates of Graphene-Ag Nanohole Arrays Fabricated by Sub-Diffraction Plasmonic Lithography. *OSA Contin* **2019**, *2* (3), 582.
(47) Huttunen, M. J.; Rasekh, P.; Boyd, R. W.; Dolgaleva, K. Using Surface Lattice Resonances to Engineer Nonlinear Optical Processes in Metal Nanoparticle Arrays. *Phys. Rev. A* **2018**, *97* (5), 053817.
(48) Juodenas, M.; Tamulevičius, T.; Henzie, J.; Erts, D.; Tamulevičius, S. Surface Lattice Resonances in Self-Assembled Arrays of Monodisperse Ag Cuboctahedra. *ACS Nano* **2019**, *13* (8), 9038−9047.
(49) Esteban, R.; Taylor, R. W.; Baumberg, J. J.; Aizpurua, J. How Chain Plasmons Govern the Optical Response in Strongly Interacting Self-Assembled Metallic Clusters of Nanoparticles. *Langmuir* **2012**, *28* (24), 8881−8890.
(50) Törmä, P.; Huttunen, M. J.; Dolgaleva, K.; Boyd, R. W. Ultra-Strong Polarization Dependence of Surface Lattice Resonances with out-of-Plane Plasmon Oscillations. *Opt. Express* **2016**, *24* (25), 28279−28289.
(51) Charconnet, M.; Kuttner, C.; Plou, J.; García-Pomar, J. L.; Mihi, A.; Liz-Marzán, L. M.; Seifert, A. Mechanically Tunable Lattice-Plasmon Resonances by Templated Self-Assembled Superlattices for Multi-Wavelength Surface-Enhanced Raman Spectroscopy. *Small Methods* **2021**, *5* (10), 2100453.
(52) Ragheb, I.; Braïk, M.; Lau-Truong, S.; Belkhir, A.; Rumyantseva, A.; Kostcheev, S.; Adam, P. M.; Chevillot-Biraud, A.; Lévi, G.; Aubard, J.; et al. Surface Enhanced Raman Scattering on Regular Arrays of Gold Nanostructures: Impact of Long-Range Interactions and the Surrounding Medium. *Nanomaterials* **2020**, *10* (11), 2201.
(53) Weitz, D. A.; Garoff, S.; Gramila, T. J. Excitation Spectra of Surface-Enhanced Raman Scattering on Silver-Island Films. *Opt. Lett.* **1982**, *7* (4), 168.
(54) Félidj, N.; Aubard, J.; Lévi, G.; Krenn, J. R.; Hohenau, A.; Schider, G.; Leitner, A.; Aussenegg, F. R. Optimized Surface-Enhanced Raman Scattering on Gold Nanoparticle Arrays. *Appl. Phys. Lett.* **2003**, *82* (18), 3095−3097.
(55) Haynes, C. L.; Van Duyne, R. P. Plasmon-Sampled Surface-Enhanced Raman Excitation Spectroscopy. *J. Phys. Chem. B* **2003**, *107* (30), 7426−7433.
(56) McFarland, A. D.; Young, M. A.; Dieringer, J. A.; Van Duyne, R. P. Wavelength-Scanned Surface-Enhanced Raman Excitation Spectroscopy. *J. Phys. Chem. B* **2005**, *109* (22), 11279−11285.
(57) Chew, H.; Wang, D.-S.; Kerker, M. Surface Enhanced Raman Scattering (SERS) by Molecules Adsorbed at Spherical Particles. *Appl. Opt.* **1980**, *19* (19), 3373−3388.
(58) Kumar, S.; Tokunaga, K.; Namura, K.; Fukuoka, T.; Suzuki, M. Experimental Evidence of a Twofold Electromagnetic Enhancement Mechanism of Surface-Enhanced Raman Scattering. *J. Phys. Chem. C* **2020**, *124* (38), 21215−21222.
(59) Tao, A.; Sinsermsuksakul, P.; Yang, P.; Tao, A.; Sinsermsuksakul, P.; Yang, P. Polyhedral Silver Nanocrystals with Distinct Scattering Signatures. *Angew. Chem. Int. Ed* **2006**, *45*, 4597−4601.
(60) Juodėnas, M.; Khinevich, N.; Klyvis, G.; Henzie, J.; Tamulevičius, T.; Tamulevičius, S. Lasing in an Assembled Array of Silver Nanocubes. *Nanoscale Horiz.* **2024**, *10*, 142−149.
(61) Ni, S.; Isa, L.; Wolf, H. Capillary Assembly as a Tool for the Heterogeneous Integration of Micro- and Nanoscale Objects. *Soft Matter* **2018**, *14* (16), 2978−2995.
(62) Li, M.; Liu, D.; Wei, D. D.; Song, X.; Wei, D. D.; Wee, A. T. S. Controllable Synthesis of Graphene by Plasma-Enhanced Chemical Vapor Deposition and Its Related Applications. *Advanced Science* **2016**, *3* (11), 1600003.
(63) Zhou, H.; Yu, W. J.; Liu, L.; Cheng, R.; Chen, Y.; Huang, X.; Liu, Y.; Wang, Y.; Huang, Y.; Duan, X. Chemical Vapour Deposition Growth of Large Single Crystals of Monolayer and Bilayer Graphene. *Nat. Commun.* **2013**, *4* (1), 1−8.
(64) Shivayogimath, A.; Whelan, P. R.; MacKenzie, D. M. A.; Luo, B.; Huang, D.; Luo, D.; Wang, M.; Gammelgaard, L.; Shi, H.; Ruoff, R. S.; et al. Do-It-Yourself Transfer of Large-Area Graphene Using an Office Laminator and Water. *Chem. Mater.* **2019**, *31* (7), 2328−2336.
(65) Tamulevičius, T.; Šeperys, R.; Andrulevičius, M.; Kopustinskas, V.; Meškinis, Š.; Tamulevičius, S.; Mikalayeva, V.; Daugelavičius, R. Application of Holographic Sub-Wavelength Diffraction Gratings for Monitoring of Kinetics of Bioprocesses. *Appl. Surf. Sci.* **2012**, *258* (23), 9292−9296.
(66) Mazet, V. Background correction. *Annu. Rep. Anal. At. Spectrosc.* **1983**, *13*, 52−54.
(67) Juodėnas, M.; Peckus, D.; Tamulevičius, T.; Yamauchi, Y.; Tamulevičius, S.; Henzie, J.; Henzie, J. Effect of Ag Nanocube Optomechanical Modes on Plasmonic Surface Lattice Resonances. *ACS Photonics* **2020**, *7* (11), 3130−3140.
(68) Hwangbo, Y.; Lee, C. K.; Mag-Isa, A. E.; Jang, J. W.; Lee, H. J.; Lee, S. B.; Kim, S. S.; Kim, J. H. Interlayer Non-Coupled Optical Properties for Determining the Number of Layers in Arbitrarily Stacked Multilayer Graphenes. *Carbon* **2014**, *77*, 454−461.
(69) Wang, H.; Wang, Y.; Cao, X.; Feng, M.; Lan, G. Vibrational Properties of Graphene and Graphene Layers. *J. Raman Spectrosc.* **2009**, *40* (12), 1791−1796.
(70) Jorio, A. Raman Spectroscopy in Graphene-Based Systems: Prototypes for Nanoscience and Nanometrology. *International Scholarly Research Notices* **2012**, *2012*, 234216.
(71) Monshi, M.; Moussavi, M.; Peckus, D.; Rajackaitė, E.; Vasiliauskas, A.; Andrulevičius, M.; Tamulevičius, T.; Tamulevičius, S. Correlation Study of Graphitic Shell Encapsulated Nickel: A Multi-Spectroscopic Approach. *Carbon* **2025**, *232*, 119704.
(72) Agarwal, N. R.; Lucotti, A.; Tommasini, M.; Neri, F.; Trusso, S.; Ossi, P. M. SERS Detection and DFT Calculation of 2-

Naphthalene Thiol Adsorbed on Ag and Au Probes. *Sens Actuators B Chem.* **2016**, *237*, 545−555.
(73) Son, J.; Kim, G. H.; Lee, Y.; Lee, C.; Cha, S.; Nam, J. M. Toward Quantitative Surface-Enhanced Raman Scattering with Plasmonic Nanoparticles: Multiscale View on Heterogeneities in Particle Morphology, Surface Modification, Interface, and Analytical Protocols. *J. Am. Chem. Soc.* **2022**, *144* (49), 22337−22351.
(74) Yaghobian, F.; Korn, T.; Schüller, C. Frequency Shift in Graphene-Enhanced Raman Signal of Molecules. *ChemPhysChem* **2012**, *13* (18), 4271−4275.
(75) Arshad, F.; Nabi, F.; Iqbal, S.; Khan, R. H. Applications of Graphene-Based Electrochemical and Optical Biosensors in Early Detection of Cancer Biomarkers. *Colloids Surf. B Biointerfaces* **2022**, *212*, 112356.
(76) Karton, A. π-π Interactions between Benzene and Graphene by Means of Large-Scale DFT-D4 Calculations. *Chem. Phys.* **2022**, *561*, 111606.
(77) Lechner, C.; Sax, A. F. Adhesive Forces between Aromatic Molecules and Graphene. *J. Phys. Chem. C* **2014**, *118* (36), 20970−20981.
(78) Yoon, J. C.; Thiyagarajan, P.; Ahn, H. J.; Jang, J. H. A Case Study: Effect of Defects in CVD-Grown Graphene on Graphene Enhanced Raman Spectroscopy. *RSC Adv.* **2015**, *5* (77), 62772−62777.
(79) Smith, R. S.; Kay, B. D. Desorption Kinetics of Benzene and Cyclohexane from a Graphene Surface. *J. Phys. Chem. B* **2018**, *122* (2), 587−594.
(80) Chakradhar, A.; Sivapragasam, N.; Nayakasinghe, M. T.; Burghaus, U. Adsorption Kinetics of Benzene on Graphene: An Ultrahigh Vacuum Study. *Journal of Vacuum Science & Technology A: Vacuum, Surfaces, and Films* **2016**, *34* (2), 021402.

https://doi.org/10.1021/acs.jpcc.5c02135
J. Phys. Chem. C 2025, 129, 14983−14992